Research Article

Protein Expression of STRO-1 Cells in Response to Different Topographic Features

Fahsai Kantawong,[1] Mary E. Robertson,[2] Nikolaj Gadegaard,[2] Richard O. C. Oreffo,[3] Richard J. Burchmore,[4] and Matthew J. Dalby[5]

[1] *Division of Clinical Chemistry, Department of Medical Technology, Faculty of Associated Medical Sciences, Chiang Mai University, Chiang Mai 50200, Thailand*

[2] *Centre for Cell Engineering, Department of Electronics and Electrical Engineering, Rankine Building, University of Glasgow, Glasgow G12 8QQ, UK*

[3] *Bone and Joint Research Group, Centre for Human Development, Stem Cells and Regeneration, Institute of Developmental Sciences, DOHAD, University of Southampton, Medical School, Southampton S016 6YD, UK*

[4] *Sir Henry Welcome Functional Genomics Facility, Institute of Biomedical and Life Sciences, Joseph Black Building, University of Glasgow, Glasgow G12 8QQ, UK*

[5] *Centre for Cell Engineering, Division of Biochemistry and Cell Biology, Institute of Biomedical and Life Sciences, Joseph Black Building, University of Glasgow, Glasgow G12 8QQ, UK*

Correspondence should be addressed to Fahsai Kantawong, air252009@gmail.com

Human skeletal stem cells (STRO-1 positive) display distinct responses to different topographical features. On a flat surface, skeletal cells spread, and *in vitro*, they typically display a polarized, fibroblast-like morphology. However, on microgrooved surfaces, these cells prefer to stretch along the grooves forming a similar morphology to *in vivo*, bipolarized fibroblasts. In contrast, on nanopits, these cells display a polygonal and osteoblastic phenotype. We have examined mechanotransduction events of STRO-1 positive in response to fibroblastic, microgrooved and osteogenic, controlled disorder nanopit, topographies using proteomics after 3 days in culture. Protein expression profiles were analyzed by difference gel electrophoresis to identify proteins that showed modulation of expression in response to different topographic features to assess early decision events in these cells on these discrete topographies. After only 72 hours in culture, STRO-1 positive displayed differential regulations of families of proteins involved in cell migration and proliferation. The current study indicated that osteogenic decision specific events had already occurred. Runx2 was localized in nuclei of the skeletal stem cells on the osteogenic nanopits; however, few signaling pathway changes were observed. This study demonstrated that micro- and nanotopographies activated skeletal stem cells at different times and with distinct mechanotransduction profiles.

1. Introduction

Topography presents powerful cues to cells effecting adhesion, migration, proliferation, and differentiation as an important factor during morphogenesis and influences the efficiency of other cues [1–3]. Ever since Clark et al. described contact guidance through cell elongation along μm features and showed that cells react to lines of discontinuity in the substratum by actin nucleation [3–5], the role of the cytoskeleton and cell attachments to substratum topography has been investigated using various microscope methods [6–9]. Changes in cell morphology happens in concert with changes in actin and tubulin cytoskeleton [1]; for example, the aggregation of actin along groove/ridge boundaries determined cells orientation on microgrooved substrata [5]. Additionally, it was found that microtubule functions in maintaining the cell shape and polarity are mediated by motor proteins [10].

Subsequently, changes in gene expression were noted on micro- and nanotopographical surfaces in the areas of cell signaling, proliferation, cytoskeleton, and production of extracellular matrix (ECM) proteins [11, 12]. These studies were supported by the study on small GTP-binding proteins of the Rho family, which revealed their involvement in the organization of cell actin cytoskeleton [13]. It is also noted that Rac GTP-binding proteins are implicated in the dynamic organization of the actin cytoskeleton [14]. Cytoskeletal changes will be driven by modulation of cell adhesion through cell surface receptors which the cytoskeleton is connected. Integrins are important receptors for cell adhesion to ECM proteins such as fibronectin and laminin.

As discussed, the adhesion of cells to topographic features generates transmembrane signals that affect cell proliferation, differentiation, and survival. Understanding signaling pathway events triggered by topography is now a focus of much research activity, and most of this research focuses on transcription events (e.g., using PCR or microarray). The focus of proteomics may be more apt, as the expression of the proteins is the ultimate expression of cell phenotype. Furthermore, proteomic investigation can provide candidate proteins for more in-depth investigation.

In the present study, a temporal protein expression profile of STRO-1 skeletal stem cell response to topography substratum was examined using proteomics (difference in gel electrophoresis—mass spectroscopy). The topographical surfaces were chosen to either align the cells (grooves) or to induce osteogenic differentiation from the stem cells (near-square patterns) [15].

Flagged changes in protein regulation were related to signal transduction pathways. The fitting of the data into pathways suggests a correlation with the morphogenic events occurring during adhering to different topographic features.

2. Materials and Methods

2.1. Material Fabrication

2.1.1. Microgroove Topography. Quartz slides were cleaned in 7 parts sulphuric acid and 1 part hydrogen peroxide for 5 mins. The slides were then spincoated with AZ primer (SHOFU INC, Japan) at 4,000 rpm for 30 secs. Shipley S1818 photoresist (Shipley Company, Mass, USA) was next added, and the slides were spun at 4,000 rpm for a further 30 secs. After spinning, the slides were soft baked at 90°C for 30 mins. The samples were then exposed to UV light through a chrome mask (Hoya), patterned with a $12.5\,\mu m$ wide line pattern. The exposed resist was developed using $1:1$ (v/v) Shipley AZ developer: water. The slides were next etched to produce $2\,\mu m$ deep grooves in a Plasma Technology RIE80 unit (Tri-chloromethane environment, pressure of 15 mTorr (1 Torr = 133.322 Pa), R.F. power of 100 W, giving an etch rate of 25 nm/min). The mastering resist was then removed and the whole slide was etched for a further minute to produce a uniform chemistry. The fabricated slide has $12.5\,\mu m$ width and $2\,\mu m$ depth microgrooved topography.

2.1.2. Disordered Nanopit (NSQ50). Samples were made by electron beam lithography (EBL). Silicon substrates were coated with ZEP-520A resist (5,000 rpm) to a thickness of 100 nm. After the samples were baked for a few hours at 180°C, they were exposed in a Leica LBPG 5-HR100 beamwriter at 50 kV. We have developed an efficient way to pattern a $1\,cm^2$ area with 1–10 billion pits [16]. An 80 nm spot size was used, finally resulting, after embossing, in pits with a diameter of 120 nm. The pitch between the pits was set to an average of 300 nm with a ± 50 nm error (in x and y) written into the placement of the pits at the centre of the square. After exposure, the samples were developed in *o*-xylene at 23°C for 60 s and rinsed in copious amounts of *iso*-2-propanol. Nickel dies were made directly from the patterned resist samples. A thin (50 nm) layer of Ni-V was sputter coated on the samples. This layer acted as an electrode in the subsequent electroplating process. The dies were plated to a thickness of ca. $300\,\mu m$.

Polymeric replicas were made in PCL (Sigma-Aldrich) sheets either against the silicon masters for NSQ50 or against the original quartz slides for the grooves. A PCL sheet was cut into $1.5\,cm^2$ squares before being cleaned with 75% ethanol followed by deionized water and blown dry with cool air. The PCL substrates were heated on hot plate at 60°C until they started to melt. Either the NSQ50 nickel shim or grooved/planar slides were embossed onto the PCL substrates. The PCL substrates were cooled down, and the moulds were removed. Grooved substrate and its control were made with areas of $1.5\,cm^2$, whilst NSQ50 and its control were made with areas of $1\,cm^2$. Three replicas of each substrate were used for each experiment.

2.2. Cell Culture. Human bone marrow stromal cells were obtained from hematologically normal patients undergoing routine surgery. Only tissue that would have been discarded was used with the approval of the Southampton and South West Hants Local Research Ethics Committee (LREC 194/99). Primary cultures of bone marrow cells were established as previously described [17]. The STRO-1+ fraction was isolated according to our previously published protocol [18].

STRO-1+ cells (P2) were cultured in $75\,cm^2$ tissue culture flasks. Culture was maintained in basal media (α-MEM containing 10% FBS and 2% antibiotics) at 37°C, supplemented with 5% CO_2. Confluent cell sheets were trypsinized and 1×10^5 cells were seeded onto embossed or control PCL. Materials were cultured in basal medium and maintained in culture with 5% CO_2 at 37°C for 3 days. At least, three replicates of material types (flat, grooved, and NSQ50) were used in each experiment to meet the statistic criteria.

2.3. Cell Morphology. After 3 days, cell morphology was observed by Coomassie staining. PCL sheets with cultured cells were fixed in 4% formaldehyde in PBS for 5 minutes. Cell staining was then performed using 5% Coomassie blue in 40% methanol and 10% acetic acid for 5 minutes. The stained materials were washed twice in tap water. Cell morphology was viewed by bright field microscopy (Zeiss)

with an objective 10x lens NA = 0.25 (Leica). Pictures were taken by greyscale digital camera (Scion Corporation Model CFW-1310M).

2.4. Difference Gel Electrophoresis

2.4.1. Protein Extraction. After 3 days culture, cells were lysed in 1 mL of DIGE lysis buffer (7 M Urea, 2 M Thiourea, 4% 3-[(3-Cholamidopropyl)dimethylammonio]-1-propanesulfonate (CHAPS) and 30 mM Tris-base pH 8.0) with 1X final concentration of general purposes protease inhibitor cocktail (Sigma-Aldrich). The cell suspension was left at room temperature for 1 hour with vigorous mixing every 20 minutes. The PCL samples were taken out, and the suspension was then centrifuged at 2,100 rpm for 10 minutes to remove insoluble material. Proteins were then precipitated from the supernatant by addition of 4 volumes of 100% cold acetone. After centrifugation, the protein pellets were washed in 80% acetone and resuspended in DIGE lysis buffer. The Bradford protein assay was used to determine the amount of protein extracted from each material. Briefly, varying concentrations of BSA (50, 25, 12.5, 6.25, and 3.125 μg/mL) were prepared and used as a standard curve. 10 μL of each standard and sample was mixed with 200 μL of protein assay reagent (Bio-Rad). The reaction was left to progress at room temperature for 5 minutes. Absorbance was measured at 595 nm. Concentrations of the protein extract from the test materials were determined from the standard curve. Protein extracts were evaluated by DIGE and DeCyder software as explained in Figure 1.

2.4.2. Saturation Labeling. 5 μg of the extracted proteins were added into sterile microfuge tubes. Protein in each tube was reduced with 1 μL of 2 mM *tris*(2-carboxyethyl)phosphine (TCEP). The reactions were incubated at 37°C in the dark for 1 hour. Protein in each tube was labelled with the required volumes (2 μL) of Cy3 and Cy5 in the dark for 30 minutes (Typically, 5 μg of protein requires 2 nmol TCEP and 4 nmol of CyDye). Equal volumes of 2X sample buffer (7 M Urea, 2 M Thiourea, 4% w/v CHAPS, 2% w/v IPG buffer pH 4–7 and 2% w/v DTT) were added to stop the reactions. Proteins labelled with Cy3 and Cy5 were mixed together. 2D electrophoresis was then performed.

2.4.3. 2D-Gel Electrophoresis. First-dimension isoelectric focusing (IEF) was performed on IPG strips (24 cm; linear gradient pH 4–7) using an Ettan IPGphor system (GE-Healthcare). IEF was performed using the following voltage program: 30 V constant for 12 h, 300 V constant for 1 h, linear up to 600 V over 1 h, linear up to 1,000 V over 1 h, linear up to 8,000 V over 3 h, then 8,000 V constant for 8.5 h. The current was limited to 50 μA *per* strip and the temperature maintained at 20°C. After focusing, strips were equilibrated for 15 min in 5 mL of reducing solution (6 M urea, 100 mM Tris-HCl pH 8, 30% v/v glycerol, 2% w/v SDS, 5 mg/mL DTT). For second-dimension SDS-PAGE, IPG strips were placed on the top of 12% acrylamide gels cast in low fluorescence glass plates and then sealed by 0.5% (w/v) agarose overlay solution. Gels were run at constant
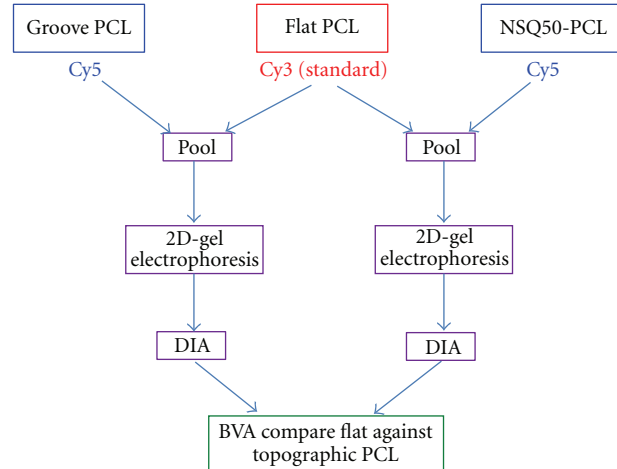

FIGURE 1: Working diagram: this diagram presented how protein extracts from flat and topographic surfaces were evaluated by DIGE and DeCyder software.

power 50 Watt/gel until the bromophenol blue tracking front had reached the base of the gel. Fluorescence images of the gels were obtained by scanning on a Typhoon 9400 scanner (GE Healthcare). Cy3 and Cy5 images were scanned at 532 nm/580 nm and 633 nm/670 nm excitation/emission wavelengths, respectively, at a 100 μm pixel size resolution. Image analysis and statistical quantification of relative protein expression was performed using DeCyder 7 software (GE Healthcare). 1.8-fold cutoff was used to determine up- or downregulation of protein spots. Statistical significance was determined by unpaired t-test which is part of the software, a P value of 0.05 was considered significant compared to protein expression of cells cultured on flat control surfaces.

2.4.4. Preparative 2D Gel. 500 μg protein extracted from human STRO-1+ cultured in a tissue culture flask was reduced by 10 μL of 20 mM TCEP and then labelled with 10 μL of 20 mM Cy3 DIGE fluorophore. After this, 2D-gel electrophoresis was performed and the gel scanned as described above. The preparative gel image was matched with analytical DIGE gel images and the spots of interest were selected for further analysis. A pick list was generated, containing gel coordinates that were used to direct spot cutting for spots of interest. Gel spots were excised using an Ettan Spot Handling Workstation (Amersham Biosciences, UK), and each gel piece was placed in a separate well of a 96-well plate. Gel pieces were washed three times in 100 μL of 50 mM ammonium bicarbonate, 50% v/v methanol, and then twice in 100 μL 75% v/v acetonitrile, before drying. Gel pieces were rehydrated with trypsin solution (20 μg trypsin/mL 20 mM ammonium bicarbonate) and incubated for 4 h at 37°C. Peptides were extracted from the gel pieces by washing twice in 100 μL of 50% v/v acetonitrile/0.1% v/v trifluoroacetic acid, before being transferred in solution to a fresh 96 well plate and dried before mass spectrometric (MS) analysis.
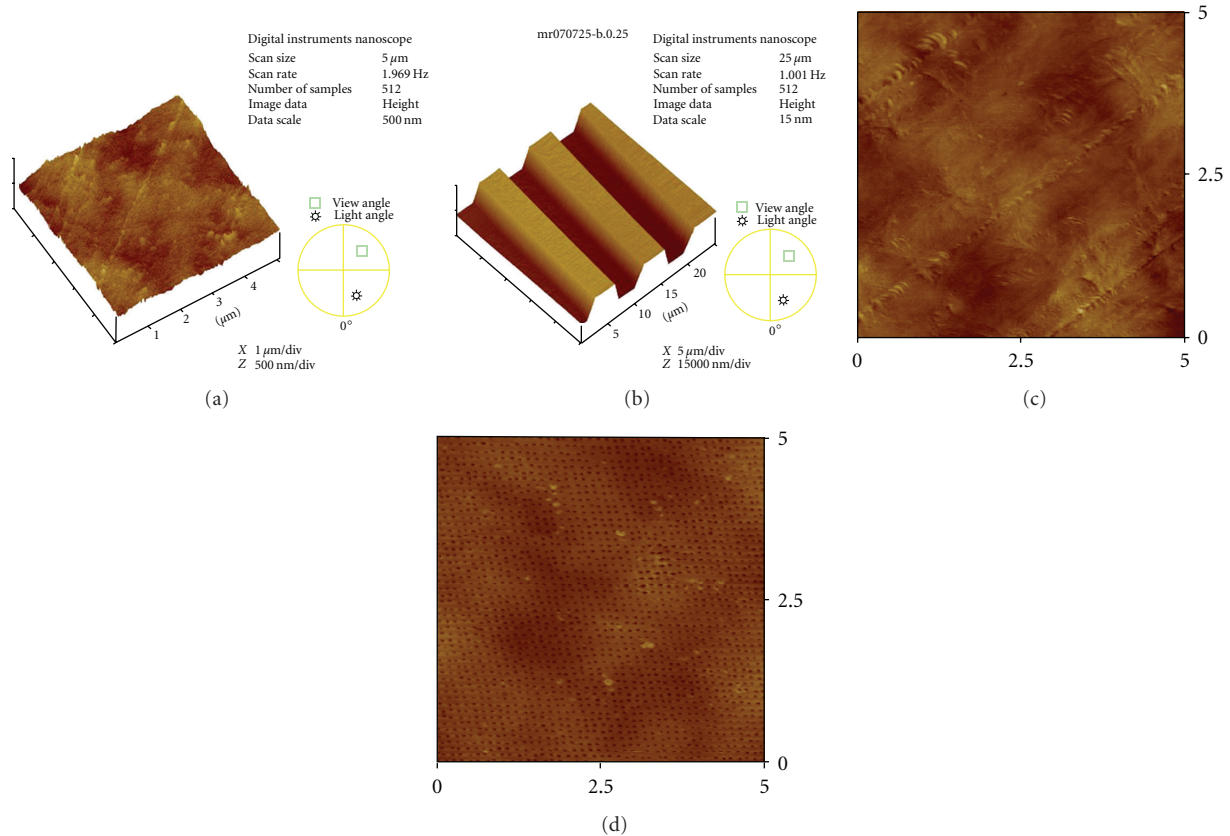
FIGURE 2: Atomic force microscope analysis: topographic features were successfully transferred onto the PCL sheets: (a) control flat PCL surface viewed at the same scale as grooved surface, (b) grooved PCL, (c) control flat PCL surface viewed at the same scale as nanopit surface, and (d) disordered nanopit surface (NSQ50).

2.4.5. MS/MS and Database Analysis. Tryptic peptide solutions were mixed at a 1 : 1 ratio with 5 mg/mL α-cyano-4-hydroxycinnamic acid (CHCA) matrix in 0.3% TFA, and spotted on stainless steel MALDI sample plates (Applied Biosystems, Framingham, MA). Peptide mixtures were then analyzed using MALDI/TOF/TOF (4700 Proteomics Analyzer, Applied Biosystems, Framingham, MA). MALDI-TOF spectra were collected from m/z 800–4000 and up to 10 peaks were selected for MS/MS analysis. Protein identification was performed using Global Proteome Server Explorer software (Applied Biosystems, Framingham, Mass, USA) utilizing the NCBI Reference Sequence human protein database. Protein identifications were assigned using the Mascot search engine, which gives each protein a probability based molecular weight search (MOWSE) score. In all cases variable methionine oxidation was used for searches. Only proteins identified with a significant score ($P \leq 0.05$) were included, corresponding to a MOWSE score greater than 66.

2.5. Immunofluorescence Staining. The osteogenic investigation was followed after 4 days of culture. The cells on the test materials were fixed in 4% formaldehyde/PBS, with 1% sucrose at 37°C for 15 min. When fixed, the samples were washed with PBS, and a permeabilising buffer (10.3 g sucrose, 0.292 g NaCl, 0.06 g $MgCl_2$, 0.476 g Hepes buffer,

0.5 mL Triton X, in 100 mL water, pH 7.2) was added at 4°C for 5 min. The samples were then incubated at 37°C for 5 min in 1% BSA/PBS, followed by the addition of an antirunx2 primary antibody (1 : 50 in 1% BSA/PBS, monoclonal anti-human raised in mouse) for 1 h at 37°C. Simultaneously, rhodamine conjugated phalloidin (Molecular Probes, Oregon, USA) was added for the duration of this incubation (1 : 100 in 1% BSA/PBS). The samples were next washed in 0.5% Tween 20/PBS (5 min × 3). A secondary, biotin conjugated antibody, (1 : 50 in 1% BSA/PBS, monoclonal horse antimouse (IgG), Vector Laboratories, Peterborough, UK) was added for 1 h (37°C) followed by washing. A FITC conjugated streptavidin third layer was added (1 : 50 in 1% BSA/PBS, Vector Laboratories, Peterborough, UK) at 4°C for 30 min, and given a final wash. Samples were then viewed by fluorescence microscopy (Zeiss Axiovert 200 m).

3. Results

3.1. Cell Morphology. The topographies were imprinted into PCL substrates with good fidelity (Figure 2). After 3 days culture on these topographic surfaces, human STRO-1+ cells on the flat control were observed to display a distinct and well spread morphology as visualised by Coomassie blue staining. Cells on microgrooved PCL were observed to display a
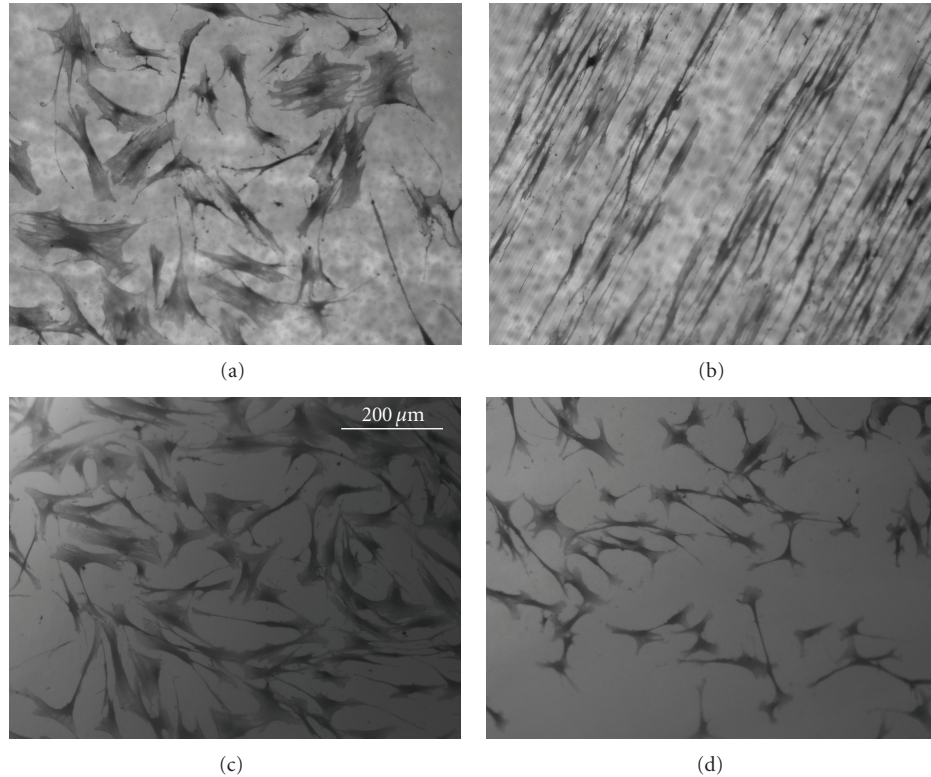
FIGURE 3: Cell morphology: (a) control flat PCL sheet, (b) grooved PCL, (c) control flat PCL sheet, and (d) disordered nanopits (NSQ50). Cells displayed a spread morphology on flat surface (a) and (c). On the grooved surface, they aligned along grooves (b), whilst on NSQ50 cells were contracted (d).

distinct bipolar morphology and to be stretched along the grooved direction of the microtopography, whilst polygonal cells were observed on NSQ50 (Figure 3).

3.2. Difference Gel Electrophoresis (DIGE). DIGE results indicate that the expression of 17 identified spots were significantly modulated following the culture of human STRO-1+ cells on microgrooved PCL and NSQ50 compared to those cultured on flat control (Table 1). These proteins were identified from the reference gels (a typical gel is presented in Figure 4). The functional relationship between the proteins is displayed in Figure 5.

3.3. Runx2. Immunofluorescent staining of Runx2 was performed after 4 days culture on control flat PCL, microgrooved PCL, and nanopit PCL (Figure 6). Runx2 was observed in cells on control (flat PCL sheet) at cell edge and bipolar cells on microgrooved PCL sheet. However, Runx2 localization was observed in the nucleus of cells cultured on the osteogenic NSQ50.

4. Discussion

This study has shown the ability of discrete topographical cues to modulate the skeletal stem cell proteome after only 72 hours in culture on microgrooved surface. We observed change of 17 protein spots including: laminin binding

protein, nucleophosmin1 (NPM1), annexin A5 (ANX5), 14-3-3 family, myosin light chain2 (MYL2) isoforms, tubulin, eukaryotic translation elongation factor1 (eEF1), Hsp90, tropomyosin1, tropomyosin2, tropomyosin3, tropomyosin4, and Rho GDP-dissociation inhibitor (RhoGDI). These proteins are implicated in cell survival, proliferation, and migration indicated heightened proliferative activity of cells on the microgrooved surface as presented in Figure 5. To follow osteogenic activity, Runx2 localization was investigated the following day, and this showed that the transcription factor Runx2 expression was observed throughout the cell but intensively accumulated at cell edge on flat PCL. Runx2 was found in the inner part of cells cultured on grooved PCL whilst Runx2 was located centrally in cells maintained on NSQ50. Runx2 is important, as it is a multifunctional transcription factor that controls skeletal development by regulating the differentiation of chondrocytes and osteoblasts and the expression of many extracellular matrix protein genes during differentiation [19, 20]. The dynamic shuttling of RUNX factors in living cells is important for gene regulation [21]. Previous study demonstrated that osteo-adipo progenitors expressed transcription factor RUNX2 and when cultured in osteogenic medium, RUNX2 moved to the nucleus and the cells differentiated to osteocytes [22].

This correlates well with our previous observations of osteogenesis on NSQ50 at longer culture times [2, 23]. However, as the proteomic proliferation profile is decreased

TABLE 1: Protein expression profiles: protein expression profile of cells cultured on grooved PCL compared against flat PCL is presented in column A. Protein expression profile of cells cultured on NSQ50 compared against flat PCL is presented in column B. Three replicates of DIGE analysis were performed. Average volume (AV) ratios of protein expression together with P values are presented. The numbers of proteins were related to the numbers in the preparative gel image. Change of protein expressions and statistical significance were determined by the DeCyder 7 software, P value 0.05 was considered significant compared to protein expression on flat surface.

| No.	Protein	A Micro-groove versus Flat		B Nanopits versus Flat	
		AV ratio	t-test (P value)	AV ratio	t-test (P value)
1	Laminin binding protein	+2.00	0.001	−1.21	0.54
2	Nucleophosmin1 (NPM1)	+1.91	0.067	−1.09	0.42
3	Annexin A5 (ANX5)	+3.63	0.002	+1.05	0.32
4	14-3-3zeta	+2.68	0.007	+1.02	0.43
5	14-3-3epsilon	+2.32	0.009	−1.01	0.40
6	14-3-3gamma	+2.29	0.008	+1.17	0.60
7	Myosin light chain2 (MYL2) isoform1	+2.3	0.017	+1.14	0.645
8	MYL2 isoform2	+2.15	0.157	+1.53	0.116
9	MYL2 isoform3	+3.74	0.002	+1.26	0.058
10	Tubulin	+2.39	0.000	+1.03	0.51
11	Eukaryotic translation elongation factor1 (eEF1)	+2.20	0.003	+1.58	0.057
12	Hsp90	+4.14	0.090	−1.00	0.55
13	Tropomyosin1	+2.32	0.011	−2.01	0.095
14	Tropomyosin2	+2.40	0.041	−2.00	0.08
15	Tropomyosin3	+1.67	0.01	−1.50	0.10
16	Tropomyosin4	+1.74	0.11	−1.79	0.042
17	Rho GDP-dissociation inhibitor (RhoGDI)	+3.24	0.007	+1.34	0.54
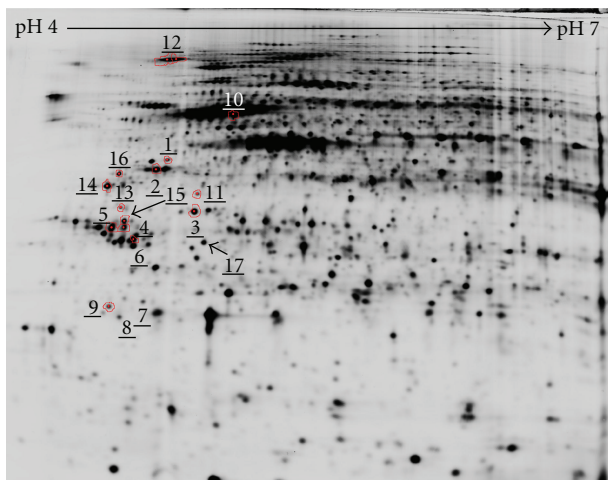
FIGURE 4: DIGE analysis: proteins with changed expression were presented on DIGE preparative gel image. The numbers represented proteins with changes in their expression, that is, 1 Laminin binding protein, 2 Nucleophosmin, 3 AnnexinV, 4 14-3-3zeta, 5 14-3-3epsilon, 6 14-3-3gamma, 7 Myosin light chain, 8 Myosin light chain, 9 Myosin light chain, 10 Tubulin, 11 eEF1, 12 Hsp90, 13 Tropomyosin1, 14 Tropomyosin2, 15 Tropomyosin3, 16 Tropomyosin4, and 17 RhoGDI.

in cells on NSQ50, it can be postulated that the proliferation of skeletal stem cells on NSQ50 was decreased as osteogenic activity was increased even after such a short time in culture.

To consider the identified proteins in more detail, it has been previously reported that laminin-332 induces an osteogenic phenotype in human skeletal or mesenchymal stem cells (hMSCs) via a focal adhesion kinase (FAK) and ERK-related pathways which are triggered via the alpha3 LG3 integrin-binding domain of laminin-332 [24]. This binding activated FAK and ERK leading to activation of the osteogenic transcription factor Runx2 and expression of key osteogenic markers [19, 20, 25]. However, this binding did not increase matrix mineralization [24]. Upregulation of laminin binding protein in this study could modulate FAK. FAK is an essential nonreceptor tyrosine kinase for regulating cell migration, adhesive signaling, and mechanosensing. FAK has been implicated in enhancing integrin activation to promote ligand binding and, hence, the strength of adhesion [26]. The effect of ERK on proliferation and differentiation is a complex issue. At first, with modest levels of activation, it will enhance proliferation; however, it will eventually slow proliferation and "switch on" transcription factors related to osteogenesis [15]. Several studies show evidence that adhesion modulation driven by laminin binding induces Rho signaling, PI3K/Akt and ERK1/2 pathways providing a possible mechanostransduction mechanism as presented in Figure 6 [27–30].

The Rho signaling pathway also plays a crucial role in cell proliferation and cell migration. RhoGDI (Rho GDP-dissociation inhibitor) regulates Rho subfamily GTPases [31]. Overexpression of RhoGDI in HT29 cells resulted in a
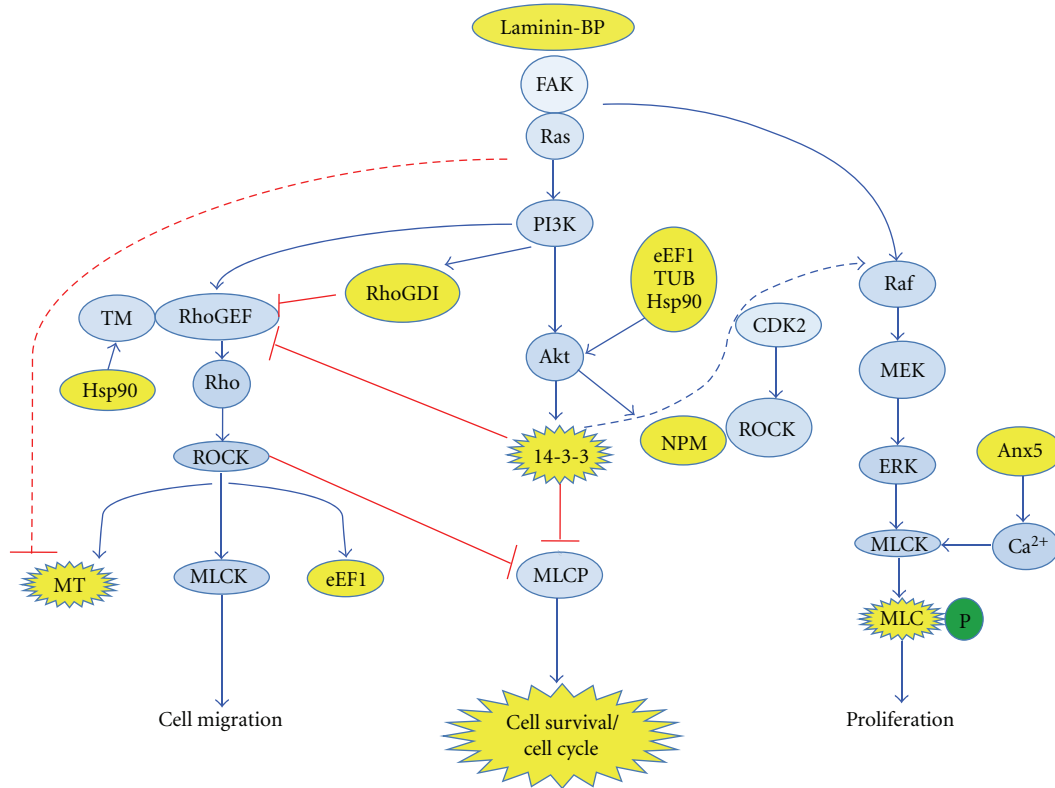
FIGURE 5: Signaling schematic representation: The postulated signaling pathway involved in this study. Proteins with significant change in their expressions are highlighted yellow.
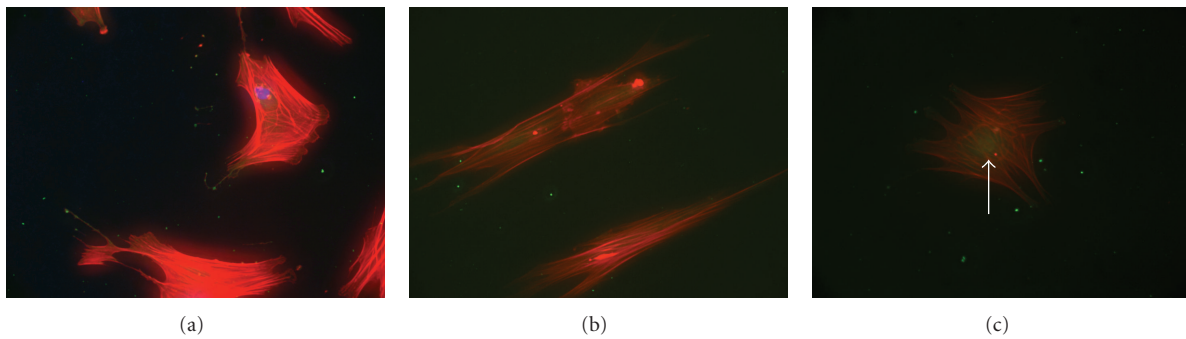

(a)   (b)   (c)

FIGURE 6: Runx2 staining: Runx2 expression was observed throughout the cell but intensively accumulated at cell edge on flat PCL (a). Runx2 was found in the inner part of cells cultured on grooved PCL (b), whilst Runx2 expression was located centrally in cells maintained on NSQ50 (c). Arrow shows Runx 2 localization.

significant increase in cell proliferation and motility *in vitro* [32].

Upregulation of the 14-3-3 family can refer to the activation of PI3K/Akt, ERK and Rho signaling pathways. Many studies reported 14-3-3 as Akt substrates [33–35] and that 14-3-3 binds to GEF Rho has been reported [36–38]. 14-3-3beta overexpression inhibits myosin light-chain phosphatase (MLCP) activity via the interaction with Myosin phosphatase target subunit 1 (MYPT1) and 14-3-3 dissociates MLCP from myosin II attenuating MLCP activity [39]. Myosin light chain kinase (MLCK) functions downstream of ERK to promote cellular migration [40].

In addition, nucleophosmin (NPM)/B23 influences Rho kinase II (ROCK II). The ROCK isoforms are downstream targets of Rho which mediate different cellular functions [41]. A previous study indicated that ROCK II is the effecter of the CDK2/cyclin E-NPM/B23 pathway involved in cell proliferation [42]. Thus, upregulation of nucleophosmin in this study supported that cells were proliferating. Furthermore, ROCK has been intimately linked to skeletal stem cell differentiation [43, 44].

The tropomyosin family of cytoskeletal proteins is implicated in stabilizing actin microfilaments [45, 46]. In a migrating cell, a subset of microtubules becomes stabilized

[47]. The molecular chaperone Hsp90, which is essential for the folding and activity of numerous client proteins involved in cell proliferation and apoptosis, associates with the microtubule network [48]. Upregulation of these proteins could be involved with mechanical tension in cells. Furthermore, annexin A5 (Anx5) upregulation supports these observations. The upregulation of Anx5 in this study may provide cells with a mechanism by which cellular responses to mechanical force (or mechanical confinement in the case of topography) might be amplified and regulated [49].

Finally, the upregulation of eukaryotic protein elongation factor 1 (eEF1) supported that cells on microgrooves were proliferating. eEF1 is modulated by PI3K [50] and the Rho/Rho-kinase pathway [51].

As discussed, Runx2 is an essential transcription factor for osteoblast differentiation [52]. The expression of Runx2 is regulated by many factors, for example, bone morphogenetic protein-2 (BMP-2) [53] and core-binding factor-beta (Cbf beta) which is required for DNA binding of Runx2 [54]. Phosphoinositide 3-kinase (PI3K)-Akt signaling enhances DNA binding of Runx2 and Runx2-dependent transcription. Runx2 upregulates PI3K subunits and Akt. Therefore, Runx2 and PI3K-Akt signaling depend on each other in the regulation of osteoblast and chondrocyte differentiation [19, 25].

From previous work, we know that certain microgrooves induce fibroblast formation from skeletal stem cell enriched (STRO-1) populations [55] and that NSQ50 topography results in osteoblastic, bone differentiation [15]. In this study, increased Runx2 staining is seen on the NSQ50 nanopits compared to the elongated, bipolar (*in vivo* fibroblast-like) cells on the microgrooves and the polarized, (*in vitro* fibroblast-like) cells on planar control (Figures 3 and 6). The signal schematic derived from our DIGE data (Figure 5) associated with cell proliferation, migration, and survival and pathways significantly modulated by the cells cultured on the microgrooves. These features of cell behavior are likely desirable for fibroblasts migrating along, for example, collagen fibers involved in, for example, wound healing rather than progenitor bone cell differentiation. Thus, the observation that these processes are mainly downregulated on the NSQ50 topography indicates, as would be expected, that less motile and less proliferative cells are differentiating towards the osteogenic lineage. Furthermore, the observed Runx2 localization suggests that the key osteogenic signal transduction processes [19, 25] have already occurred by day 4 or that a global proteomic approach is not sensitive enough to detect such changes. The current studies indicate the need for the use of strategies that will employ a compartmentalized approach to protein isolation or a temporal study of early time points to delineate the signal transduction processes in osteoblast differentiation.

5. Conclusion

In conclusion, these studies underline the importance of nanotopographical and microtopographical cues in delineating bone cell signal transduction and the importance of a temporal approach to understanding cell signaling and the implications therein from the current data in further functional studies to modulate bone formation critical in the development of reparative strategies for an ageing population.

References

[1] M. J. Dalby, S. Childs, M. O. Riehle, H. J. Johnstone, S. Affrossman, and A. S. Curtis, "Fibroblast reaction to island topography: changes in cytoskeleton and morphology with time," *Biomaterials*, vol. 24, no. 6, pp. 927–935, 2003.

[2] M. J. Dalby, N. Gadegaard, R. Tare et al., "The control of human mesenchymal cell differentiation using nanoscale symmetry and disorder," *Nature Materials*, vol. 6, no. 12, pp. 997–1003, 2007.

[3] P. Clark, P. Connolly, A. S. Curtis, J. A. Dow, and C. D. Wilkinson, "Topographical control of cell behaviour. I. Simple step cues," *Development*, vol. 99, no. 3, pp. 439–448, 1987.

[4] P. Clark, P. Connolly, and G. R. Moores, "Cell guidance by micropatterned adhesiveness in vitro," *Journal of Cell Science*, vol. 103, no. 1, pp. 287–292, 1992.

[5] B. Wojciak-Stothard, A. S. Curtis, W. Monaghan, M. McGrath, I. Sommer, and C. D. Wilkinson, "Role of the cytoskeleton in the reaction of fibroblasts to multiple grooved substrata," *Cell Motility and the Cytoskeleton*, vol. 31, no. 2, pp. 147–158, 1995.

[6] M. J. Dalby, L. Di Silvio, G. W. Davies, and W. Bonfield, "Surface topography and HA filler volume effect on primary human osteoblasts in vitro," *Journal of Materials Science*, vol. 11, no. 12, pp. 805–810, 2000.

[7] T. N. Opara, M. J. Dalby, E. J. Harper, L. Di Silvio, and W. Bonfield, "The effect of varying percentage hydroxyapatite in poly(ethylmethacrylate) bone cement on human osteoblast-like cells," *Journal of Materials Science*, vol. 14, no. 3, pp. 277–282, 2003.

[8] A. S. G. Curtis, M. J. Dalby, and N. Gadegaard, "Nanoprinting onto cells," *Journal of the Royal Society Interface*, vol. 3, no. 8, pp. 393–398, 2006.

[9] M. J. P. Biggs, R. G. Richards, N. Gadegaard, C. D. Wilkinson, and M. J. Dalby, "Regulation of implant surface cell adhesion: characterization and quantification of S-phase primary osteoblast adhesions on biomimetic nanoscale substrates," *Journal of Orthopaedic Research*, vol. 25, no. 2, pp. 273–282, 2007.

[10] V. I. Gelfand, F. K. Gyoeva, E. Tanaka, A. D. Bershadsky, J. M. Vasiliev, and V. I. Rodionov, "Microtubule-dependent control of cell shape and pseudopodial activity is inhibited by the antibody to kinesin motor domain," *Journal of Cell Biology*, vol. 123, no. 6, pp. 1811–1820, 1993.

[11] M. J. Dalby, S. J. Yarwood, M. O. Riehle, H. Johnstone, S. Affrossman, and A. Curtis, "Increasing fibroblast response to materials using nanotopography: morphological and genetic measurements of cell response to 13-nm-high polymer demixed islands," *Experimental Cell Research*, vol. 276, no. 1, pp. 1–9, 2002.

[12] M. J. Dalby, M. O. Riehle, S. J. Yarwood, C. D. W. Wilkinson, and A. Curtis, "Nucleus alignment and cell signaling in fibroblasts: response to a micro-grooved topography," *Experimental Cell Research*, vol. 284, no. 2, pp. 274–282, 2003.

[13] M. L. Malosio, D. Gilardelli, S. Paris, C. Albertinazzi, and I. de Curtis, "Differential expression of distinct members of rho

family GTP-binding proteins during neuronal development: identification of RAC1B, a new neural- specific member of the family," *Journal of Neuroscience*, vol. 17, no. 17, pp. 6717–6728, 1997.

[14] C. Albertinazzi, A. Cattelino, and I. de Curtis, "Rac GTPases localize at sites of actin reorganization during dynamic remodeling of the cytoskeleton of normal embryonic fibroblasts," *Journal of Cell Science*, vol. 112, no. 21, pp. 3821–3831, 1999.

[15] F. Kantawong, K. E. Burgess, K. Jayawardena et al., "Whole proteome analysis of osteoprogenitor differentiation induced by disordered nanotopography and mediated by ERK signalling," *Biomaterials*, vol. 30, no. 27, pp. 4723–4731, 2009.

[16] N. Gadegaard, S. Thoms, D. S. MacIntyre et al., "Arrays of nano-dots for cellular engineering," *Microelectronic Engineering*, vol. 67-68, pp. 162–168, 2003.

[17] X. B. Yang, H. I. Roach, N. M. Clarke et al., "Human osteoprogenitor growth and differentiation on synthetic biodegradable structures after surface modification," *Bone*, vol. 29, no. 6, pp. 523–531, 2001.

[18] S. M. Howdle, K. A. Partridge, X. Yang et al., "Immunoselection and adenoviral genetic modulation of human osteoprogenitors: in vivo bone formation on PLA scaffold," *Biochemical and Biophysical Research Communications*, vol. 299, no. 2, pp. 208–215, 2002.

[19] T. Fujita, Y. Azuma, R. Fukuyama et al., "Runx2 induces osteoblast and chondrocyte differentiation and enhances their migration by coupling with PI3K-Akt signaling," *Journal of Cell Biology*, vol. 166, no. 1, pp. 85–95, 2004.

[20] T. Komori, "Regulation of bone development and extracellular matrix protein genes by RUNX2," *Cell and Tissue Research*, vol. 339, no. 1, pp. 189–195, 2010.

[21] K. S. Harrington, A. Javed, H. Drissi et al., "Transcription factors RUNX1/AML1 and RUNX2/Cbfa1 dynamically associate with stationary subnuclear domains," *Journal of Cell Science*, vol. 115, no. 21, pp. 4167–4176, 2002.

[22] Y. Lin, W. Jing, L. Wu et al., "Identification of osteo-adipo progenitor cells in fat tissue," *Cell Proliferation*, vol. 41, no. 5, pp. 803–812, 2008.

[23] F. Kantawong, R. Burchmore, N. Gadegaard, R. O. Oreffo, and M. J. Dalby, "Proteomic analysis of human osteoprogenitor response to disordered nanotopography," *Journal of the Royal Society Interface*, vol. 6, no. 40, pp. 1075–1086, 2009.

[24] R. F. Klees, R. M. Salasznyk, D. F. Ward et al., "Dissection of the osteogenic effects of laminin-332 utilizing specific LG domains: LG3 induces osteogenic differentiation, but not mineralization," *Experimental Cell Research*, vol. 314, no. 4, pp. 763–773, 2008.

[25] T. Komori, "Mechanism of transcriptional regulation by Runx2 in osteoblasts," *Clinical Calcium*, vol. 16, no. 5, pp. 801–807, 2006.

[26] K. E. Michael, D. W. Dumbauld, K. L. Burns, S. K. Hanks, and A. J. García, "Focal adhesion kinase modulates cell adhesion strengthening via integrin activation," *Molecular Biology of the Cell*, vol. 20, no. 9, pp. 2508–2519, 2009.

[27] M. Andjelkovic, D. R. Alessi, R. Meier et al., "Role of translocation in the activation and function of protein kinase B," *Journal of Biological Chemistry*, vol. 272, no. 50, pp. 31515–31524, 1997.

[28] Y. Baba, K. I. Iyama, K. Hirashima et al., "Laminin-332 promotes the invasion of oesophageal squamous cell carcinoma via PI3K activation," *British Journal of Cancer*, vol. 98, no. 5, pp. 974–980, 2008.

[29] Y. G. Wang, X. Ji, M. Pabbidi, A. M. Samarel, and S. L. Lipsius, "Laminin acts via focal adhesion kinase/phosphatidylinositol-3′ kinase/protein kinase B to down-regulate beta1-adrenergic receptor signalling in cat atrial myocytes," *Journal of Physiology*, vol. 587, no. Pt 3, pp. 541–550, 2009.

[30] A. Watson, V. L. Morris, and B. M. Chan, "Coordinated integrin and growth factor regulation of primary keratinocyte migration mediated through extracellular signal regulated kinase and phosphoinositide 3-kinase," *Archives of Dermatological Research*, vol. 301, no. 4, pp. 307–317, 2009.

[31] A. J. Ridley, W. E. Allen, M. Peppelenbosch, and G. E. Jones, "Rho family proteins and cell migration," *Biochemical Society Symposium*, vol. 65, pp. 111–123, 1999.

[32] L. Zhao, H. Wang, J. Li, Y. Liu, and Y. Ding, "Overexpression of Rho GDP-dissociation inhibitor atpha is associated with tumor progression and poor prognosis of colorectal cancer," *Journal of Proteome Research*, vol. 7, no. 9, pp. 3994–4003, 2008.

[33] D. W. Powell, M. J. Rane, Q. Chen, S. Singh, and K. R. McLeish, "Identification of 14-3-3zeta as a protein kinase B/Akt substrate," *Journal of Biological Chemistry*, vol. 277, no. 24, pp. 21639–21642, 2002.

[34] J. Sunayama, F. Tsuruta, N. Masuyama, and Y. Gotoh, "JNK antagonizes Akt-mediated survival signals by phosphorylating 14-3-3," *Journal of Cell Biology*, vol. 170, no. 2, pp. 295–304, 2005.

[35] N. Kakinuma, B. C. Roy, Y. Zhu, Y. Wang, and R. Kiyama, "Kank regulates RhoA-dependent formation of actin stress fibers and cell migration via 14-3-3 in PI3K-Akt signaling," *Journal of Cell Biology*, vol. 181, no. 3, pp. 537–549, 2008.

[36] A. Chahdi and A. Sorokin, "Protein kinase A-dependent phosphorylation modulates beta1Pix guanine nucleotide exchange factor activity through 14-3-3beta binding," *Molecular and Cellular Biology*, vol. 28, no. 5, pp. 1679–1687, 2008.

[37] F. Zenke, M. Krendel, C. Dermardirossian, C. C. King, B. Bohl, and G. M. Bokoch, "p21-activated kinase 1 phosphorylates and regulates 14-3-3 binding to GEF-H1, a microtubule-localized Rho exchange factor," *Journal of Biological Chemistry*, vol. 279, no. 18, pp. 18392–18400, 2004.

[38] K. Namikawa, Q. Su, S. Kiryu-Seo, and H. Kiyama, "Enhanced expression of 14-3-3 family members in injured motoneurons," *Molecular Brain Research*, vol. 55, no. 2, pp. 315–320, 1998.

[39] Y. Koga and M. Ikebe, "A novel regulatory mechanism of myosin light chain phosphorylation via binding of 14-3-3 to myosin phosphatase," *Molecular Biology of the Cell*, vol. 19, no. 3, pp. 1062–1071, 2008.

[40] D. H. Nguyen, A. D. Catling, D. Webb et al., "Myosin light chain kinase functions downstream of Ras/ERK to promote migration of urokinase-type plasminogen activator-stimulated cells in an integrin-selective manner," *Journal of Cell Biology*, vol. 146, no. 1, pp. 149–164, 1999.

[41] J. K. Liao, M. Seto, and K. Noma, "Rho kinase (ROCK) inhibitors," *Journal of Cardiovascular Pharmacology*, vol. 50, no. 1, pp. 17–24, 2007.

[42] Z. Ma, M. Kanai, K. Kawamura, K. Kaibuchi, K. Ye, and K. Fukasawa, "Interaction between ROCK II and nucleophosmin/B23 in the regulation of centrosome duplication," *Molecular and Cellular Biology*, vol. 26, no. 23, pp. 9016–9034, 2006.

[43] R. McBeath, D. M. Pirone, C. M. Nelson, K. Bhadriraju, and C. S. Chen, "Cell shape, cytoskeletal tension, and RhoA regulate stem cell lineage commitment," *Developmental Cell*, vol. 6, no. 4, pp. 483–495, 2004.

[44] K. A. Kilian, B. Bugarija, B. T. Lahn, and M. Mrksich, "Geometric cues for directing the differentiation of mesenchymal stem cells," *Proceedings of the National Academy of Sciences of the United States of America*, vol. 107, no. 11, pp. 4872–4877, 2010.

[45] V. Shah, S. Bharadwaj, K. Kaibuchi, and G. L. Prasad, "Cytoskeletal organization in tropomyosin-mediated reversion of ras-transformation: evidence for Rho kinase pathway," *Oncogene*, vol. 20, no. 17, pp. 2112–2121, 2001.

[46] H. Honda, Y. Kitano, K. Hatori, and K. Matsuno, "Dual role of tropomyosin on chemically modified actin filaments from skeletal muscle," *FEBS Letters*, vol. 383, no. 1-2, pp. 55–58, 1996.

[47] K. Onishi, M. Higuchi, T. Asakura, N. Masuyama, and Y. Gotoh, "The PI3K-Akt pathway promotes microtubule stabilization in migrating fibroblasts," *Genes to Cells*, vol. 12, no. 4, pp. 535–546, 2007.

[48] J. Giustiniani, V. Daire, I. Cantaloube et al., "Tubulin acetylation favors Hsp90 recruitment to microtubules and stimulates the signaling function of the Hsp90 clients Akt/PKB and p53," *Cellular Signalling*, vol. 21, no. 4, pp. 529–539, 2009.

[49] T. L. Haut Donahue, D. C. Genetos, C. R. Jacobs, H. J. Donahue, and C. E. Yellowley, "Annexin V disruption impairs mechanically induced calcium signaling in osteoblastic cells," *Bone*, vol. 35, no. 3, pp. 656–663, 2004.

[50] A. Amiri, F. Noei, S. E. V. Jeganathan, G. Kulkarni, D. E. Pinke, and J. Lee, "eEF1A2 activates Akt and stimulates Akt-dependent actin remodeling, invasion and migration," *Oncogene*, vol. 26, no. 21, pp. 3027–3040, 2007.

[51] T. Izawa, Y. Fukata, T. Kimura, A. Iwamatsu, K. Dohi, and K. Kaibuchi, "Elongation factor-1 alpha is a novel substrate of rho-associated kinase," *Biochemical and Biophysical Research Communications*, vol. 278, no. 1, pp. 72–78, 2000.

[52] T. Komori, "Regulation of bone development and extracellular matrix protein genes by RUNX2," *Cell and Tissue Research*, vol. 339, no. 1, pp. 189–195, 2010.

[53] S. Kato, N. Kawabata, N. Suzuki, M. Ohmura, and M. Takagi, "Bone morphogenetic protein-2 induces the differentiation of a mesenchymal progenitor cell line, ROB-C26, into mature osteoblasts and adipocytes," *Life Sciences*, vol. 84, no. 9-10, pp. 302–310, 2009.

[54] N. Kanatani, T. Fujita, R. Fukuyama et al., "Cbf beta regulates Runx2 function isoform-dependently in postnatal bone development," *Developmental Biology*, vol. 296, no. 1, pp. 48–61, 2006.

[55] F. Kantawong, K. Burgess, K. Jayawardena et al., "Effects of a surface topography composite with puerariae radix on human STRO-1-positive stem cells," *Acta Biomaterialia*, vol. 6, no. 9, pp. 3694–3703, 2010.